Available online at www.sciencedirect.com
SCIENCE DIRECT®
ELSEVIER
Nuclear Instruments and Methods in Physics Research A 551 (2005) 261–270
NUCLEAR INSTRUMENTS & METHODS IN PHYSICS RESEARCH Section A
www.elsevier.com/locate/nima

High-speed particle tracking in nuclear emulsion by last-generation automatic microscopes

N. Armenise[a], M. De Serio[a], M. Ieva[a], M.T. Muciaccia[a], A. Pastore[a], S. Simone[a], J. Damet[b,1], I. Kreslo[b], N. Savvinov[b], T. Waelchli[b], L. Consiglio[c], M. Cozzi[c], D. Di Ferdinando[c], L.S. Esposito[c], G. Giacomelli[c], M. Giorgini[c], G. Mandrioli[c], L. Patrizii[c], M. Sioli[c], G. Sirri[c], L. Arrabito[d], I. Laktineh[d], P. Royole-Degieux[d], S. Buontempo[e], N. D'Ambrosio[e], G. De Lellis[e], G. De Rosa[e], F. Di Capua[e], D. Coppola[e], F. Formisano[e], A. Marotta[e], P. Migliozzi[e], C. Pistillo[e], L. Scotto Lavina[e], G. Sorrentino[e], P. Strolin[e], V. Tioukov[e], F. Juget[f], M. Hauger[f], G. Rosa[g], E. Barbuto[h], C. Bozza[h,*], G. Grella[h], G. Romano[h], C. Sirignano[h]

[a]*Università degli Studi di Bari and INFN, Bari, Italy*
[b]*Bern University, Bern, Switzerland*
[c]*Università di Bologna and INFN, Bologna, Italy*
[d]*IPNL, IN2P3-CNRS and Universitè C. Bernard, Lyon, Villeurbanne, France*
[e]*Università "Federico II" and INFN, Napoli, Italy*
[f]*Neuchâtel University, Neuchâtel, Switzerland*
[g]*Università "La Sapienza" and INFN, Roma, Italy*
[h]*Università di Salerno and INFN, Italy*

Received 10 May 2005; accepted 20 June 2005
Available online 25 July 2005

Abstract

The technique of nuclear emulsions for high-energy physics experiments is being revived, thanks to the remarkable progress in measurement automation achieved in the past years. The present paper describes the features and performances of the *European Scanning System*, a last-generation automatic microscope working at a scanning speed of

*Corresponding author. INFN-Dipartimento di Fisica, Università di Salerno, via S. Allende, 84081 Baronissi (Sa), Italy. Tel.: +39 089965420; fax: +39 089965275.
E-mail address: kryss@sa.infn.it (C. Bozza).
[1]Now at LAPP, IN2P3-CNRS and Universitè de Savoie, Annecy, France.

doi:10.1016/j.nima.2005.06.072

$20\,cm^2/h$. The system has been developed in the framework of the OPERA experiment, designed to unambigously detect $\nu_\mu \to \nu_\tau$ oscillations in nuclear emulsions.

PACS: 29.40.Rg; 29.40.Gx; 07.05.Pj

Keywords: Nuclear emulsions; Automatic scanning; Digital imaging; Microscopy; ν oscillations; Elementary particles

1. Introduction

Nuclear emulsions have been among the earliest particle detectors used in high-energy physics [1]. They are made of a gel with interspersed AgBr crystals. A particle crossing an emulsion layer ionises the medium along its path, leaving what is called a *latent image*, i.e. a sequence of *sensitized* sites. After development, each site will act as a crystallisation nucleus for metallic Ag, and a sequence of aligned silver grains, with a linear size of $\sim 0.6\,\mu m$, will mark the path of the ionising particle in the emulsion. Typically, a minimum ionising particle leaves about 30 grains in $100\,\mu m$.

Nuclear emulsions are analysed by means of optical microscopes: adjusting the focal plane of the objective lens through the whole thickness of the emulsion allows to obtain an optical *tomography* of each field of view, and therefore to reconstruct 3D particle tracks. A full data-taking task can span several tomographic sequences of adjacent views.

Large-scale emulsion-based detectors require the development of fast automatic scanning systems.

The European Scanning System (ESS [2]), described in the present paper, has been developed in the framework of the OPERA experiment [3].

OPERA will use a large amount of emulsions[1], corresponding to a total surface to be scanned of a few thousands of m^2 in five years' run, to obtain an unambigous signature of $\nu_\mu \to \nu_\tau$ oscillations in the parameter region indicated by atmospheric neutrino data [4], using the *CERN to Gran Sasso* ν_μ beam (CNGS [5]). The detector, located in the underground Gran Sasso National Laboratories, consists of electronic trackers, iron spectrometers and a massive lead-emulsion target, segmented into *bricks* with size $12.7 \times 10.2 \times 7.5\,cm^3$. Each brick is a sequence of lead plates and emulsion foils, made of two $43\,\mu m$ thick films on either side of a $200\,\mu m$ plastic base.

Thanks to the excellent tracking resolution of nuclear emulsion ($<1\,\mu m$), the short-lived τ particles produced in ν_τ charged current interactions occurring in lead can be directly observed and the *appearance* of ν_τ's in an almost pure ν_μ beam can be investigated.

OPERA was conceived after the success of automatic scanning in the CHORUS experiment [6], where the technique of automatic track recognition by means of computer-controlled microscopes, namely the *Track Selector* [7] and the *SySal* system [8], has been first applied to a large sample of events.

The ESS project takes its inspiring ideas from the *SySal* system, developed by the University of Salerno (Italy).

The ESS is being specifically optimised for the scanning of *thin* emulsions exposed to perpendicularly impinging particles. The goals are *high* speed (more than a factor of 20 better than in the past), sub-micron precision, *high* tracking efficiency and *low* instrumental background.

The following sections describe how these goals have been successfully achieved.

The general structure of the system and the algorithms developed for image processing and particle tracking are presented here in details. The hardware, its performances and the system capabilities to reconstruct tracks and interaction vertices in OPERA bricks, using cosmic ray muons for the inter-calibration of emulsion sheets [9], will be described in future papers.

[1]The OPERA emulsion foils are being produced by Fuji Film, Minamiashigara, 250-0193, Japan.

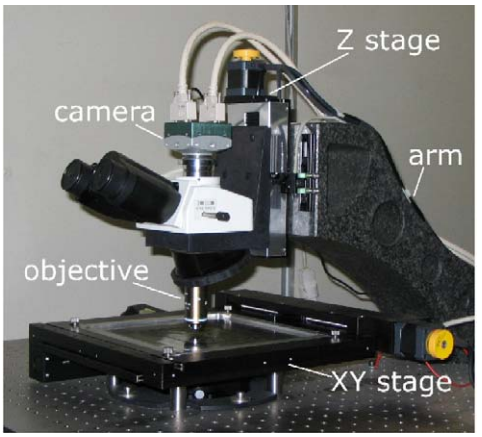

Fig. 1. The European Scanning System microscope.

2. System overview

The system uses a software-based approach for data processing. This approach has proven extremely flexible and effective, since new algorithms can be easily tested and the integration of commercial components has been possible. Therefore, the system can be quickly upgraded as technological improvements become available.

The system consists of a microscope (Fig. 1) equipped with a computer-controlled motorized stage, movable in the horizontal X–Y plane and in the vertical Z direction, a dedicated optical system and a CMOS camera, mounted on top of the optical tube. For each field of view, several images of the emulsion are taken at equally spaced depth levels. Images are grabbed and processed by a vision processor board, hosted in the control PC together with the motor control board.

2.1. Hardware configuration

The hardware components of the system are briefly described here. A detailed description of the hardware and its performances will be given in a paper in preparation.

The mechanical stage, developed in collaboration with MICOS[2], is equipped with nano-step motors (VEXTA[3] 5-phase) and optical encoders with a resolution of 0.1 μm. The motors are driven by a National Instruments[4] controller (PCI-7344) interfaced with the PCI bus. The stage has a travel range of 20 cm on the horizontal axes and 5 cm on the vertical axis. The X–Y stage takes about 125 ms for a 300 μm-step, settling time included; the positioning reproducibility is about 0.3 μm.

A modified optical bench hosts the illumination system and is equipped with a granite arm carrying the Z stage and the optical system.

The optical train has been developed in collaboration with NIKON-Italia[5] and has been designed to reproduce the performances of standard microscopes used to observe small biological specimens.

The illumination system consists of a lamphouse and a condenser (WD 4.2 mm, NA 0.85) whose positions can be adjusted with micrometric precision to operate under conditions of Köhler illumination. The observation system includes a trinocular tube, mechanically assembled to fit to the Z stage, and a $50\times$ CFI Plan Achromat oil-immersion objective (WD 0.4 mm, NA 0.9). The system is infinity corrected and produces achromatic planar images through the whole thickness of the emulsion.

The image is formed on a CMOS camera (Mikrotron[6] MC1310), used at 376 fps, with sensor resolution of 1280×1024 pixels. The resulting size of one field of view is $390\times310\,\mu m^2$.

Images are grabbed and processed using a Matrox[7] Odyssey frame grabber/vision processor.

The system runs under Microsoft Windows 2000/XP[8] on a dual processor (3 GHz) computer.

2.2. Software structure

The operations to be executed for each field of view are listed below:

- grab several images at different depths (local *tomography*),

[2] http://www.micos.ws.
[3] http://www.orientalmotor.it.
[4] http://www.ni.com.
[5] http://www.nikon.it.
[6] http://www.mikrotron.de.
[7] http://www.matrox.com.
[8] http://www.microsoft.com.

- recognise black spots (*clusters* of dark pixels) in each image,
- select possible track *grains*,
- reconstruct 3D sequences of aligned grains,
- extract a set of relevant parameters for each sequence.

Image grabbing is performed while the objective is moving along the optical axis (Z-axis). In order to obtain still pictures, an electronic shutter limits the camera integration time. The integration time currently used is $1/6000$ s, with the camera operating at 376 fps.

The pitch of the tomographic sequence depends on the *effective* depth of field, due to the optical system and to the image processing. Given the 43 μm thickness of OPERA emulsion layers, 15 pictures per view are taken in steps of about 3 μm. With a sensor of 1280×1024 pixels and 256 grey levels (8 bits per pixel), the data rate is 470 MB/s.

The implementation of a synchronous data-taking scheme is relatively simple, but the use of available resources would not be optimised: every step could act as a bottleneck; furthermore, the CPU would be idle while waiting for the cycle to be completed.

A significant improvement in terms of speed has been obtained after the implementation of an asynchronous data-taking scheme that allows parallel execution of several tasks. Execution proceeds along four independent *threads* that are synchronised at the end of each cycle:

- thread A moves the optical system along the vertical axis during the grabbing; at the end of the image taking, it resets the Z-axis position and moves the X and Y axes to the next field of view;
- thread B acquires images via the frame grabber;
- thread C is responsible for image processing; processed images are stored in a temporary memory buffer;
- thread D loads the processed images from the previous field of view and performs cluster and track recognition.

Thread A runs on the motor controller, which has its own multi-threading operating system. Threads B and C run on the Matrox Odyssey. Thread D runs on the control PC and can be split into two or more threads to exploit the power of multi-processor machines.

In principle, only threads A and B need synchronisation: provided enough memory is available, threads C and D could be indefinitely slower. In fact, with a data rate of 470 MB/s, the memory would be quickly saturated. Moreover, threads C and D happen to be much faster than A and B and a feedback response from image analysis is needed before moving the stage to the next field of view.

The grabbing stroke has to be kept within the emulsion thickness during acquisition. In order to discriminate in-emulsion levels from out-of-emulsion levels, at the end of each cycle the profile of the number of clusters as a function of depth is analysed. If a *drift* along the vertical axis is detected, the Z position is adjusted accordingly. The response of the focusing check acts as a synchronisation signal for the following cycle.

Fig. 2 shows the time diagram of a typical data-taking cycle. Presently, one cycle lasts 180 ms: image grabbing (15 layers in 43 μm) takes 55 ms, 125 ms are used to move the stage to the next field of view (about 300 μm step) and wait for X–Y

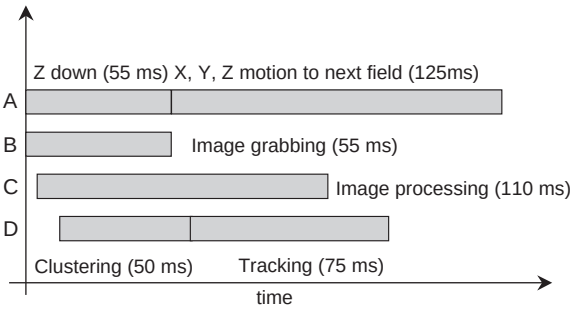

Fig. 2. Time diagram of a typical data-taking cycle. The letters on the left indicate the threads that perform the various operations (see text). Images are processed as soon as they are taken, but processing is slower than grabbing. Therefore, cluster recognition and tracking run on the images taken during the *previous* field of view. The time actually needed for these two operations depends on the number of grains in the image, thus average values are shown. The time for X, Y, Z motion includes X–Y oscillation damping and Z-axis acceleration for constant speed motion during the image grabbing.

oscillations to damp below a tolerated level of 0.2 μm.

Through a detailed study of the timing of each operation and a careful design of the system, the goal of an unprecedented scanning speed (20 cm^2/h) has been achieved. A further improvement in terms of speed may be obtained by reducing the settling time of the X–Y stage, by increasing the number of CPUs in the host PC and by the use of parallel processing for faster image handling.

3. Image processing

Grains belonging to particle tracks are normally drowned in a sea of random background grains (fog), produced during the development process. Moreover, emulsion images have several *defects*, such as scratches on the external surfaces, stains, etc., to be taken into account in image processing. Furthermore, since the grain size is ~0.6 μm, it is necessary to deal with diffractive optics. This requires a complex image treatment in order to obtain a high grain detection efficiency and an adequate rejection power of background clusters.

CMOS sensors are faster than other technologies, but normally have a high noise level: in the conversion from analogue output to digital grey level, each pixel has its own pedestal. This produces a *sand* effect on the image that must be minimised. Spots on the sensor surface can make some pixels *blind*, thus mimicking grains in fixed positions on all layers. A *flat-field* subtraction technique has been implemented to equalise pixel response with a pedestal map that is prepared at machine set-up time and is applied to every image before processing. The map should be re-computed time to time to account for camera aging and dust accumulation on the sensor surface.

The procedure to enhance dark spots on a light background is based on the Point Spread Function (PSF) and on the application of a Finite Impulse Response (FIR) filter [10].

The PSF $\Psi(x,y,z)$ gives the 3D distribution of the light intensity due to a point-like obstacle placed at $(0,0)$ on the focal plane $z=0$. A real image is the convolution of the PSF with the real object distribution. The resulting *grey level* is given by:

$$g(x,y,z) = \int_V I \cdot \Psi(x-\xi, y-\phi, z-\zeta) \times \rho(\xi,\phi,\zeta)\,\mathrm{d}\xi\,\mathrm{d}\phi\,\mathrm{d}\zeta$$

where ρ is the *obstacle density*, I is the light flux and the integral is carried out over the target volume.

In practice, the product $(I\Psi)$ also depends on the position in the image, because of non-constant illumination over the field of view and uncorrected aberrations in the optics. Thus, the grey level becomes

$$g(x,y,z) = \int_V I(\xi,\phi)\Psi(\xi,\phi,\zeta,x-\xi,y-\phi,z-\zeta) \times \rho(\xi,\phi,\zeta)\,\mathrm{d}\xi\,\mathrm{d}\phi\,\mathrm{d}\zeta.$$

It is theoretically possible to deconvolute the density of obstacles from the formula, and it is actually done in applications of cellular microscopy; however, in that field, the rate of images per second is several orders of magnitude lower, and the computation can take much longer than required by high-speed scanning.

On-line data processing for fast automatic scanning imposes the use of approximations.

First of all, instead of using integrals, the grey level formula can be approximated through a discrete sum over pixels and levels:

$$g(i_x,i_y,i_z) = \sum_{j_x j_y j_z} I(j_x,j_y) \times \Psi(j_x,j_y,j_z,i_x-j_x,i_y-j_y,i_z-j_z) \times \rho(j_x,j_y,j_z).$$

Then, in a rough approximation, Ψ can be factorised to reduce the problem to 2D:

$$\Psi(j_x,j_y,j_z,i_x-j_x,i_y-j_y,i_z-j_z) = \Psi_h(j_x,j_y,i_x-j_x,i_y-j_y)\,\delta_{i_z,j_z}. \quad (1)$$

To enhance the detection of grains of the expected size, a 2D FIR filter is applied to each image:

$$f(i_x,i_y,i_z) = \sum_{l_x,l_y} K(l_x,l_y)\,g(i_x+l_x,i_y+l_y,i_z)$$

where $K(l_x, l_y)$ is the filter or convolution kernel. Substitution in the filter formula yields:

$$f(i_x, i_y, i_z) = \sum_{l_x,l_y} \sum_{j_x,j_y} K(l_x, l_y) I(j_x, j_y) \times \Psi_h(j_x, j_y, i_x - j_x + l_x, i_y - j_y + l_y) \times \rho(j_x, j_y, j_z, i_z).$$

If Ψ_h and I were independent of (j_x, j_y) and if grains all had exactly the same size and shape $(\eta(j_x, j_y))$, K could be defined in such a way that

$$K(l_x, l_y) = \sum_{j_x,j_y} \Psi_h(l_x - j_x, l_y - j_y)\eta(j_x, j_y) - C.$$

The filter would then produce a peak when the kernel passes over a variation in the grey level that has the shape expected from the PSF convolution with a real grain. The constant C is such that $\sum_{l_x,l_y} K(l_x, l_y) = 0$, which makes the filtered image independent of the average gray level of the original image. However, being a linear functional, the filter is sensitive to multiplicative variations of the grey level: if the lamp output is increased by a factor α, the filter output will scale by the same factor. In order to remove this dependence, prior to the application of the filter, the grey level histogram of each image is *scaled* to a reference histogram.

The choice of the kernel size is the result of a balance between computation speed and filter selectivity. The convolution kernel that has been implemented has the following representation:

$$K = \begin{bmatrix} 1 & 1 & 1 & 1 & 1 & 1 \\ 1 & 2 & 3 & 3 & 2 & 1 \\ 1 & 3 & -13 & -13 & 3 & 1 \\ 1 & 3 & -13 & -13 & 3 & 1 \\ 1 & 2 & 3 & 3 & 2 & 1 \\ 1 & 1 & 1 & 1 & 1 & 1 \end{bmatrix}.$$

The action of the FIR filter on a typical emulsion image is shown in Fig. 3. The next step is image binarisation.

As already mentioned, due to residual uncorrected aberrations and to variations in the illumination, Ψ_h and I can change from point to point; as a consequence, the filter response can vary inside the field of view and it is not convenient to apply a fixed threshold to binarise the whole image. Since the point-to-point variation of the filter response is a reproducible feature of the microscope, it can be accounted for by applying a threshold map.

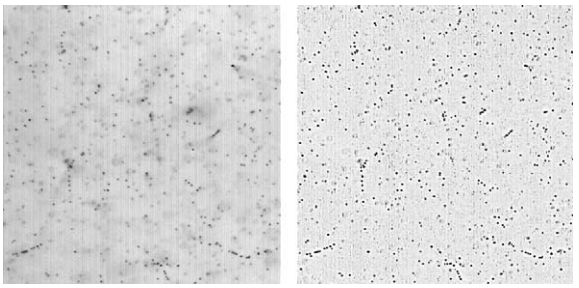

Fig. 3. A typical emulsion image (left) and effect of the FIR filter on it (right). For the sake of clarity, the image shown is a 512 × 512 excerpt from a field of view of 1280 × 1024 pixels.

At each cycle, images are binarised and transferred to the host PC memory. They are processed by a fast algorithm written in Assembler, and adjacent pixels above threshold are grouped together to form clusters. For each cluster, the position of its centre of gravity, its area and its matrix of inertia are saved.

The approximation that the PSF vanishes out of the focal plane (see Eq. (1)) fails when several clusters with identical centres of gravity are found on several consecutive tomographic levels. This effect is known as *shadowing* or *replication* and can be enhanced by the use of a weak binarisation threshold. It must be tolerated to a certain extent: indeed, grains are not localised on focal planes; if no grain is to be missed, the threshold should be weak enough that grains that are halfway between two levels should be detected at least in one of them.

4. Tracking

Normally, 1000–2000 clusters, almost all due to random background, are found in one field of view. By applying quality cuts based on shape and size, about 60% of them are typically selected and used for tracking (*grains*).

In the tomographic sequence of each field of view, as a result of the shadowing effect, *replicated* grains are found in two or more consecutive levels. However, it is not possible to simply discard them, since this would result in the partial cancellation of vertical tracks. Indeed, *shadows* can be used to improve the level-to-level alignment precision. As the Z-axis moves during the grabbing stroke, transverse vibrations can arise. An overall misalignment among the tomographic levels is thus produced. This effect can be recovered by searching for patterns of replicated grains and by applying a mapping procedure to compute the global translation of each level with respect to the previous one. The typical distribution of displacements (Fig. 4) shows a sharp peak over a background of random matches. The peak is indeed not centred at zero and the deviation, which includes also residual misalignments in the optics and mechanics, can reach an amplitude of 0.6 μm. The tracking algorithm uses the level-to-level displacements to recover such misalignments and the unpredictable effect of vibrations.

The basic idea of the tracking algorithm is that a track is a *straight* sequence of grains lying in different levels. If two grains belonging to a real micro-track are measured in two non-adjacent levels, the pair is used as a track *hint*: other grains of the same track must lie along the line between the two. For our purposes, the algorithm must take less than 100 ms to examine 20 000 grains. Checking all possible pairs would result in an awesome combinatory, thus two tests are applied to filter good track hints:

- usually not all track slopes are physically interesting, and an angular acceptance of $\tan\theta < 1$ (θ is the angle between the track direction and the vertical direction) is commonly used;
- with an emulsion sensitivity for m.i.p. tracks of 31 grains/100 μm, the number of grains of a track in each of the two 43 μm-thick emulsion layers of OPERA sheets is distributed according to the Poisson's law with an average of about 13 grains; some *trigger* levels are defined (Fig. 5), i.e. if none of these levels has a grain along the predicted line, the track search along that line stops immediately. Hereafter, a sequence of grains measured in one 43 μm-thick emulsion layer will be referred to as a *micro-track*. Micro-tracks with fewer than 6 grains (about 1%) are not accepted.

As already mentioned, grains are not exactly localised on focal planes. As a consequence, the *true* Z-positions of the grains found in the same level are uniformly distributed around the Z-position of the level itself. In practice, the

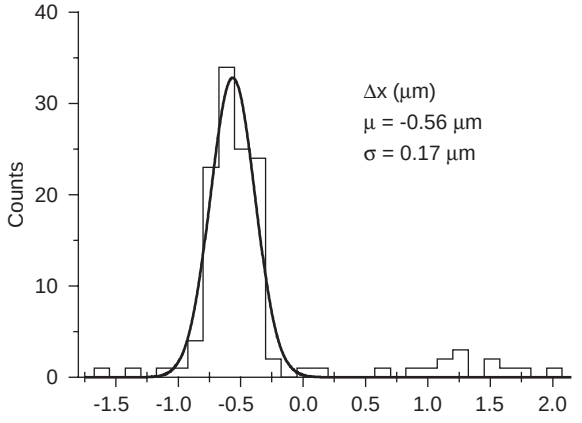

Fig. 4. Mapping of two consecutive tomographic layers using cluster *shadows*. The position differences along the X direction are shown.

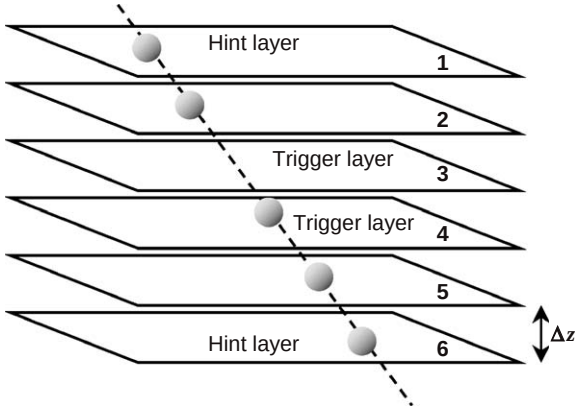

Fig. 5. A track *hint* consisting of two grains in levels 1 and 6 is shown; if the hint is confirmed in at least one of the internal trigger levels, the tracking procedure is applied to all levels.

Z-position of each single grain is known with an uncertainty Δ_z given by the sampling step.

In principle, determining whether or not any of the grains measured in a certain level belongs to a micro-track requires the evaluation of the 3D distance of a point from a straight line. In practice, since all grains lie in the same plane, the problem can be simplified to 2D, thus reducing the computation time.

A straight line representing a particle track can be parameterized as $\mathbf{I} + \alpha\mathbf{T}$, where $\mathbf{I}$ is the intercept of the track at the plane $z = z_{\text{plane}}$, $\mathbf{T} = (s_x, s_y, 1)$ is the slope vector and $\alpha = z - z_{\text{plane}}$.

If $\mathbf{S} = (s_x, s_y)$ is the projection of $\mathbf{T}$ in the horizontal plane, we can introduce the unit vector $\mathbf{n}_\parallel = (n_x, n_y)$ such that $\mathbf{S} = S\mathbf{n}_\parallel$ and its normal $\mathbf{n}_\perp = (n_y, -n_x)$; $\mathbf{n}_\parallel$ and $\mathbf{n}_\perp$ define two orthogonal directions that will be referred to as *longitudinal* and *transverse*, respectively, and denoted by the subscripts $\parallel$ and $\perp$ in the following . They define a *natural* frame for each micro-track (Fig. 6).

In this frame, the distance of a grain $\mathbf{G}$ from the track can be expressed, in the worst case, as

$$\Delta_\perp \mathbf{n}_\perp + (\Delta_\parallel + S\Delta_z)\mathbf{n}_\parallel$$

where $\Delta_\perp$ and $\Delta_\parallel$ are the transverse and longitudinal misalignments in the plane where the grain lies, as shown in Fig. 6.

At small slopes, the measurement errors along X and Y directions dominate; at large slopes, the misalignment is mainly affected by the term due to the uncertainty in Z.

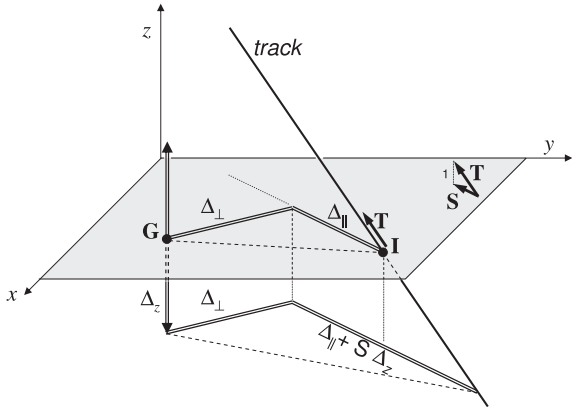

Fig. 6. In the horizontal plane, the distance of a grain $\mathbf{G}$ from the track can be decomposed along the longitudinal and transverse directions. The transverse component does not depend on the track slope.

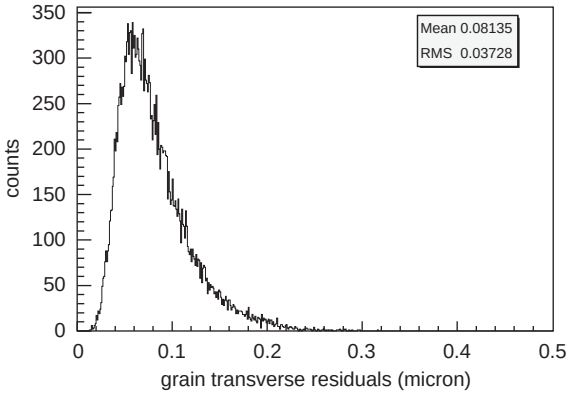

Fig. 7. Grain transverse residuals with respect to micro-track fitted trajectory (real tracks only).

Aligned grains are then selected according to transverse and longitudinal tolerances. The former, denoted as $A_\perp$, is set to 0.4 μm (Fig. 7); the latter is computed as $A_\parallel = S\Delta_z + A_\perp$.

By this choice, all the (non-Gaussian) uncertainties due to the unknown Z position are absorbed in the longitudinal component, the transverse component depending only on the (Gaussian) 2D measurement errors. The transverse alignment residuals can, therefore, be used as an estimation of the micro-track quality.

After micro-track selection, multiple reconstructions are filtered out: if a grain belongs to two or more micro-tracks, only the track with the highest number of grains is retained. Moreover, due to shadowing, it may happen that a fully independent set of replicated grains appears with fit parameters very similar to those of another micro-track. The final pass of tracking accounts for this effect and removes track duplicates.

A more reliable track reconstruction is obtained by connecting micro-tracks across the plastic base to form *base-tracks*, as shown in Fig. 8. Each micro-track is extrapolated to the corresponding Z level of the plastic support and position and slope tolerances are applied to select correlated pairs. By defining the quantity:

$$\sigma = \sqrt{\left(\frac{\Delta S_{t\perp}}{S_{\perp \text{tol}}}\right)^2 + \left(\frac{\Delta S_{t\parallel}}{S_{\parallel \text{tol}}}\right)^2}$$

$$+\sqrt{\left(\frac{\Delta S_{b\perp}}{S_{\perp tol}}\right)^2+\left(\frac{\Delta S_{b\parallel}}{S_{\parallel tol}}\right)^2}$$

where $\Delta S_{\perp(\parallel)}$ is the transverse (longitudinal) slope difference between top/bottom micro-track and base-track and $S_{\perp(\parallel)tol}$ is the corresponding tolerance ($S_{\parallel tol}=0.04+0.3\times S$, $S_{\perp tol}=0.04$), two populations emerge from the sample (Fig. 9): one with *large* σ value and a number of grains clearly incompatible with the expected Poissonian law (*fake* base-tracks, top-left), the other one with *small* σ value and a number of grains well within the Poissonian expectations (bottom-right). The cut represented by the dashed line is applied to remove the fake base-tracks.

The resulting base-track finding efficiency is above 90% over the angular range $[0,700]$ mrad and the micro-track finding efficiency is above 95%. Correspondingly, the instrumental background, estimated by visually inspecting tracks of different angles found by the automatic system, is about 1 fake base-track/cm^2.

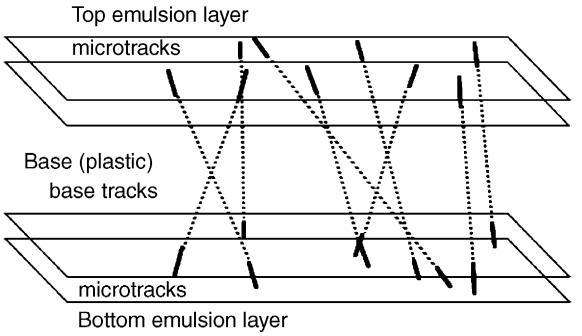

Fig. 8. Micro-track connection across the plastic base.

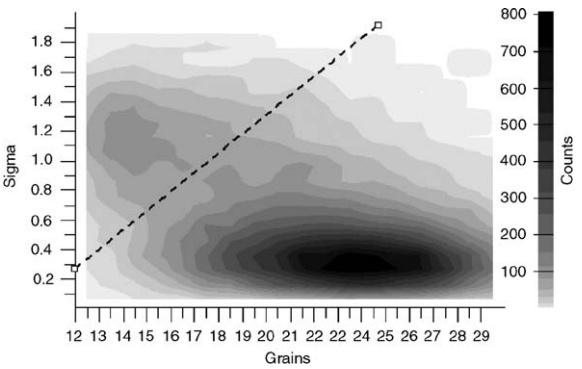

Fig. 9. Rejection of *fake* base-tracks based on both the slope agreement with the two micro-tracks (sigma, see text) and the number of grains: the cut represented by the dashed line is applied.

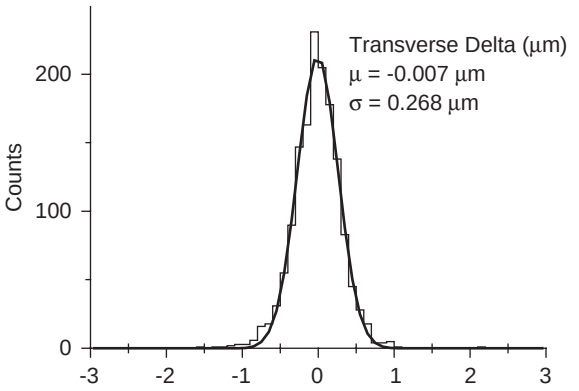

Fig. 10. Transverse position misalignment between base-tracks and corresponding fitted trajectories obtained by connecting base-tracks in consecutive emulsion sheets.

Fig. 10 shows the distribution of transverse position differences between base-tracks and corresponding fitted trajectories obtained by connecting base tracks measured in several consecutive emulsion sheets. The position misalignment, representing another estimate of track quality, is about 0.3 μm.

The quoted performances have been obtained at a scanning speed of 20 cm^2/h.

5. Conclusions

A fast automatic microscope for nuclear emulsion scanning, working at a speed of 20 cm^2/h, has been successfully developed in the framework of the *European Scanning System* project for the OPERA experiment. This system, based on the latest available hardware technologies in the fields of optics, mechanics, CMOS cameras and vision processors, is already operational in various emulsion laboratories in Europe. High-speed image analysis and tracking procedures, embedded in a complex modular software, have been developed to obtain a full *digitisation* of the information recorded in nuclear emulsion. *On-the-fly* 3D reconstruction of particle tracks is performed with

sub-micron precision, efficiency above 95% and instrumental background at the level of 1 fake track/cm^2.

The project is now evolving towards the development of a more complex system, able to detect and fully reconstruct interaction vertices in nuclear emulsion targets.

Acknowledgements

We acknowledge the cooperation of all members of the OPERA Collaboration. We gratefully acknowledge the support of the technical staff in our laboratories. In particular, we acknowledge. A Andriani, M. Di Marino and A. Ruggieri for their help in the installation and management of the automatic microscopes and E. Bottazzi, P. Di Pinto and C. Valieri for their contribution to brick assembly and emulsion processing.

References

[1] W.H. Barkas, Nuclear Research Emulsion, Academic Press, London, 1963;
C.F. Powell, P.H. Fowler, D.H. Perkins, The Study of Elementary Particles by the Photographic Method, Pergamon Press, New York, 1959.
[2] N. D'Ambrosio, et al., Nucl. Phys. B Proc. Suppl. 125 (2003) 22;
N. D'Ambrosio, Nucl. Instr. and Meth. A 525 (2004) 193.
[3] M. Guler, et al., CERN-SPSC-2000-028;
M. Guler, et al., CERN-SPSC-2001-025;
Y. Declais, et al., CERN-SPSC-2002-029.
[4] Y. Fukuda, et al., Phys. Rev. Lett. 81 (1998) 1562;
Y. Ashie, et al., Phys. Rev. Lett. 93 (2004) 101801;
M. Ambrosio, et al., Phys. Lett. B 434 (1998) 451;
M. Ambrosio, et al., Eur. Phys. J. C 36 (2004) 323;
W.W.M. Allison, et al., Phys. Lett. B 449 (1999) 137;
M. Sanchez, et al., Phys. Rev. D 68 (2003) 113004.
[5] G. Acquistapace, et al., CERN-98-02, INFN/AE-98/05 (1998);
R. Bailey, et al., CERN-SL-99-034, INFN/AE-99/05 (1999);
A.E. Ball, et al., SL-Note 2000-063 (2000).
[6] E. Eskut, et al., Nucl. Instr. and Meth. A 401 (1997) 7.
[7] S. Aoki, et al., Nucl. Instr. and Meth. B 51 (1990) 466;
S. Aoki, et al., Nucl. Instr. and Meth. A 473 (2001) 192.
[8] G. Rosa, et al., Nucl. Instr. and Meth. A 394 (1997) 357.
[9] E. Barbuto, et al., Nucl. Instr. and Meth. A 525 (2004) 485.
[10] R.C. Gonzalez, R.E. Woods, Digital Image Processing, Addison-Wesley, Reading, MA, 1993.